

# Experimental Study of Open-Wheel Race-Car Front Wings

William J. Jasinski and Michael S. Selig  
University of Illinois at Urbana-Champaign

Copyright © 1998 Society of Automotive Engineers, Inc.

## ABSTRACT

An experimental study was performed at the University of Illinois at Urbana-Champaign Low-Speed Wind Tunnel to quantify the performance and flowfield effects of two-element open-wheel race-car front wing configurations. Four distinct configurations were tested in- and out-of-ground effect and at various speeds (Reynolds numbers), angles of attack, and flap positions. A splitter plate was installed in the wind tunnel to act as the ground plane. Data presented include balance force measurements, surface pressure data, and downstream flow measurements using a seven-hole probe. Results show that these elementary factors in the design of race-car front wings have a significant effect on wing performance and behavior of the downstream flowfield.

## INTRODUCTION

**BACKGROUND** - In recent years, aerodynamics has become an increasingly important factor in the design and performance of open-wheel race cars. The large amounts of downforce produced by these cars, typically greater than two times the car's weight, allow cornering accelerations of well over 4g's. Despite recent gains made in aerodynamic design, there is still little known about the influence that race-car wings have on the production of a car's overall downforce, specifically in Champ Cars where the underbody channels produce a majority of the downforce.

Previous studies of race-car aerodynamics ranging from full-car wind-tunnel tests, numerical investigations, and combined experimental and numerical studies have shown that the effect of small changes in parameters on a race car can have significant effects on aerodynamic performance.[1,2,3] Hurst [1] shows that a 1-degree change in wheel camber, a seemingly unimportant aerodynamic variable, can change downforce by up to 2%. Katz [2] demonstrates through the use of a panel method that the addition of a front and rear wing to an open-wheel race car can change a lifting body to one that produces a large amount of downforce. These studies show that in order to use simulations as a tool to maximize performance, a race car must be modeled properly in the wind tunnel or computations.

Since it is difficult to completely match wind-tunnel conditions or numerical boundary conditions to the track conditions, tests have been performed to determine the proper way to evaluate the effect of wings on a race car. Berchak and Camosy [4] tested an isolated full-size rear wing and a 40% scale model of a vintage Indy-style car and compared results. Their study revealed that performance of the wing is enhanced by the presence of the car indicating some degree of cross-coupling between the wing and body. This idea is also supported in Refs. 2 and 3. Knowing that wing-alone results will underestimate performance when used on a race car, it is feasible to perform these tests and still be able to estimate the effects on the complete race car.

The studies mentioned above primarily deal with rear-wing aerodynamics, and there is still much to learn about how the front wing of an open-wheel race car affects performance. A series of investigations performed by Ranzenbach and Barlow [5,6,7] begin to address the performance of front wings with two-dimensional experimental and numerical methods. These studies focused mostly on the effects of the various simulations of the ground plane boundary conditions on the performance of two-dimensional airfoil sections. In the case of single-element tests of the NACA 0015 [5] and 4412 airfoils [6], comparison between experimental and computational results show fairly good agreement at ground clearances greater than 0.1 chord lengths. At lower heights, boundary layers from the airfoil and ground plane begin to interact, which becomes difficult to predict accurately with current computational methods. An additional study of a two-element airfoil (NACA 63<sub>2</sub>-215 Mod B) with a 30% slotted flap shows little agreement of absolute values of lift coefficient, but similar trends.[7] Ranzenbach and Barlow state that this discrepancy was due to problems with the experimental setup.

The tests above indicate that it is possible to perform simplified tests and still be able to extract information that is beneficial to the design of a race car despite the complexity of the overall problem.

**MOTIVATION** - Motivation for the current study surfaced because of the lack of information available on three-

dimensional downforce wings in ground effect. The flowfield near the front wing of an open-wheel race car is complicated despite being in relatively undisturbed air, although the close proximity of the wing to the front wheels tends to have a large effect on the flowfield. The current method of race-car wing design is based on trial and error: a wing is designed, a model is built and tested in the wind tunnel. If favorable results are obtained, the design is improved until the desired effect is met. The information gained from this study can help designers improve and shorten the design process by identifying crucial factors in the design of a front wing and how they affect performance before testing them in the wind tunnel. Knowledge gained from this study will be used to further enhance current design tools and verify various numerical tools that are used during the design cycle.

## EXPERIMENTAL APPARATUS

**WIND TUNNEL** - Experiments using configurations based on the UIUC700 two-element airfoil were performed at the University of Illinois at Urbana-Champaign Low-Speed Wind Tunnel. The wind tunnel is a conventional open-return type with a contraction ratio of 7.5:1 and test section dimensions of 0.853 x 1.219 m. The test section diverges approximately 1.27 cm over its 2.43-m length to allow for boundary layer growth. Flow velocity is limited to 71.52 m/s (160 mph), corresponding to a Reynolds number of approximately  $4.9 \times 10^6/m$ .

**MODEL** - Tests were performed on wing/airfoil configurations based on the UIUC700 two-element airfoil. Due to structural and space requirements, as well as available construction techniques, the UIUC700 airfoil was designed specifically for this experiment using methods described in Ref. [8] and has no relation to profiles used on actual race cars. The wind-tunnel model was tested as a semi-span wing with a span of 46.23 cm without endplates, with a main-element chord of 22.86 cm, and 2D flap having a chord of 10.16 cm, resulting in a combined reference chord length of 33.02 cm. All distances were non-dimensionalized using this chord length, independent of the flap setting. Additionally, aerodynamic forces obtained with configurations using the Champ Car front wing were non-dimensionalized using  $1654.7 \text{ cm}^2$  as the reference area, while  $1728.7 \text{ cm}^2$  was used for the Formula One front wing reference area. These reference areas are also independent of flap setting. Both the main element and 2D flap were constructed using molded carbon-fiber skins with steel bar spars. The main element had pressure taps at five spanwise locations of 10.16, 20.38, 29.49, 36.83, and 42.42 cm from the root of the wing. The 2D flap had pressure taps at three locations at 10.16, 29.49, and 42.42 cm. The taps were aligned parallel to the chord-line. The UIUC700 two-element airfoil was tested in two-dimensional flow and, when combined with a large endplate, in a configuration similar to a Champ Car rear wing. Flap deflection for these configurations could be manually set in 5 deg increments

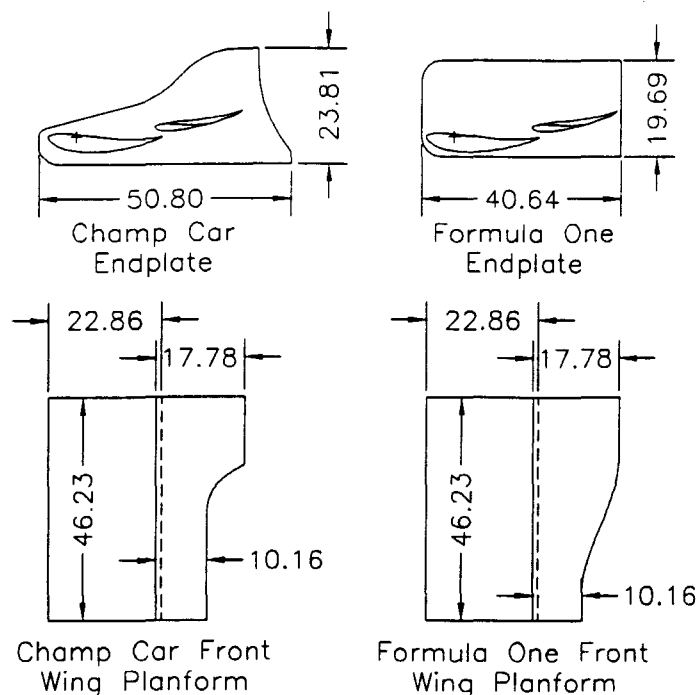


**Figure 1. Front wing and endplate planforms (in cm).**

from 6 to 41 deg. Results from these tests are beyond the scope of this paper and will not be discussed.

Two additional flaps were designed such that, when combined with the main element, would approximate the planforms of either a Champ Car or Formula One front wing planform. For these flaps, the chord increases from 10.16 cm at the root to 17.78 cm at the tip. The Champ Car flap was designed to have a long, constant root section with a sharp "cutout" that transitions into the tip, while the F1 flap design has shorter tip and root sections with a long, sweeping transition. The 3D flaps used typical foam-core construction with carbon-fiber skins and were not pressure tapped. Flap deflection, as measured at the root, was adjustable from 4 to 44 deg in 5 deg increments. Two endplates were designed to approximate the profile for either a Champ Car or Formula One front wing endplate. Each endplate could be combined with the above wing planforms to form four different front wing configurations. Front wing and endplate planforms are shown in Figure 1. A summary of the possible test configurations is given in Table 1.

**Table 1. Two-element test configurations**

| Designation | Description                  | Test | Flap  | Endplate        |
|-------------|------------------------------|------|-------|-----------------|
| UIUC700     | Two-element baseline airfoil | 2D   | "2D"  | n/a             |
| UIUC700R    | Champ Car rear wing          | 3D   | "2D"  | Champ Car rear  |
| UIUC700I    | Champ Car front wing         | 3D   | Champ | Champ Car front |
| UIUC700F    | F1 front wing                | 3D   | F1    | F1 front        |
| UIUC700G    | Hybrid front wing            | 3D   | Champ | F1 front        |
| UIUC700H    | Hybrid front wing            | 3D   | F1    | Champ Car front |

**GROUND PLANE** - To simulate ground effect, a 183 x 85.41 x 1.905-cm thick clear acrylic sheet with a full-radius leading edge was installed in the wind tunnel. The ground plane could be mounted at clearances of 302 (0.1c), 6.604 (0.2c), and 9.906-cm (0.3c). The leading edge of the ground plane was placed 66.04 cm (2c) forward of the leading edge of the main element to reduce the effects of boundary layer growth and provide for proper isolation of the wing in the tunnel. Preliminary investigations showed that at ground heights at and below 0.2c with lift coefficients greater than 2, the trailing vortex system of the wing induced boundary-layer separation on the ground plane, thereby limiting the ground clearances that could be tested. Data for ground clearance of 0.3c is the only data presented. Investigations at this height showed that wingtip vortex and ground-plane boundary-layer interaction was minimal and acceptable for the scope of this study.

**EXPERIMENTAL METHODS** - Lift, drag, and pitching moment data were acquired with a three-component external floor balance manufactured by Aerotech ATE Limited using methods as described in Refs. 9 and 10. Data were acquired at both increasing and decreasing angles of attack. Data for both directions will be shown in the results. The model was mounted to the balance so that pitching moment measurements were taken about the quarter-chord of the main element. This point was also to center of rotation to set the angle of attack. Error analysis of the balance setup indicated that errors in lift, drag, and moment coefficient were typically less than 2%. At low-speed and low-drag conditions, error in drag coefficient peaked at approximately 6%.

Downstream flowfield measurements were acquired at selected conditions using an Aeroprobe Corporation 3.175-mm diameter seven-hole probe. The probe was mounted to a two-axis traverse manufactured by Lintech, Inc. and was positioned approximately 33 cm, or one-reference chord length, behind the trailing edge of the wing. Scans included approximately 3600 individual locations with the extents and resolution that are shown in Figure 2. The upper, lower, and right boundaries of Figure 2 correspond to the wind tunnel ceiling, floor, and wall. Resolution was chosen to capture as much detail as possible in areas where large gradients in flow direction were expected while allowing for reasonable run times of approximately 2 1/2 hours. Three components of flow velocity were determined by using a combination of the seven pressures from the probe through methods outlined by Rediniotis et. al [11], as originally reported by Zilliac.[12] Measurement errors in dynamic pressure and flow angle from the seven-hole probe were typically 0.5 deg and 1%, respectively, as quoted by the manufacturer. The manufacturer provided a 1600-point calibration map, which included data for cone angles up to 70 deg. Seven-hole probe and surface pressure measurements were acquired using a Pressure Systems, Inc. 8400 pressure system with  $\pm 7$  kPa and  $\pm 35$  kPa electronic pressure scanners. Pressure scanner accuracy was quoted as 0.05% of full-scale.

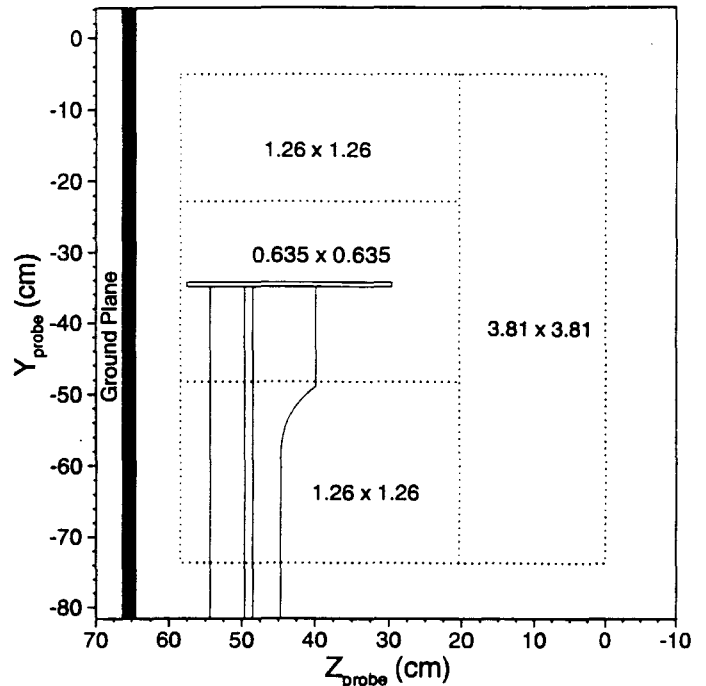


**Figure 2. Seven-hole probe scan resolution.**

**TEST MATRIX** - The test matrix was chosen to cover the effects of changing major variables of flap planform, endplate planform, angle of attack, flap deflection, and Reynolds number at a ground clearance of 9.906 cm (0.3c). Table 2 summarizes the test matrix that was performed. The four possible flap and endplate combinations formed the UIUC700I, F, G, and H configurations as described in Table 1. Due to maximum balance loads, especially at higher speeds, the number of possible flap deflections that could be tested was limited. The Reynolds number was set by varying tunnel RPM and was based on the reference chord of 33.02 cm. In the cases with the Formula One flap (UIUC700F and H), the maximum Reynolds number was lower than cases with the Champ Car flap (UIUC700G and I). This was the maximum speed that was possible without exceeding balance load ranges.

**Table 2. Front Wing Test Matrix**

| Configuration | $\alpha$ (deg) | Re                | $\delta_i$ (deg) |
|---------------|----------------|-------------------|------------------|
| UIUC700I      | -3 thru 18     | $0.7 \times 10^6$ | 14               |
| UIUC700I      | -3 thru 18     | $1.1 \times 10^6$ | 4, 14, 24        |
| UIUC700I      | -3 thru 18     | $1.3 \times 10^6$ | 14               |
| UIUC700F      | -3 thru 18     | $0.7 \times 10^6$ | 14               |
| UIUC700F      | -3 thru 18     | $1.0 \times 10^6$ | 4, 14, 24        |
| UIUC700F      | -3 thru 18     | $1.2 \times 10^6$ | 14               |
| UIUC700G      | -3 thru 18     | $0.7 \times 10^6$ | 14               |
| UIUC700G      | -3 thru 18     | $1.1 \times 10^6$ | 4, 14, 24        |
| UIUC700G      | -3 thru 18     | $1.3 \times 10^6$ | 14               |
| UIUC700H      | -3 thru 18     | $0.7 \times 10^6$ | 14               |
| UIUC700H      | -3 thru 18     | $1.0 \times 10^6$ | 4, 14, 24        |
| UIUC700H      | -3 thru 18     | $1.2 \times 10^6$ | 14               |

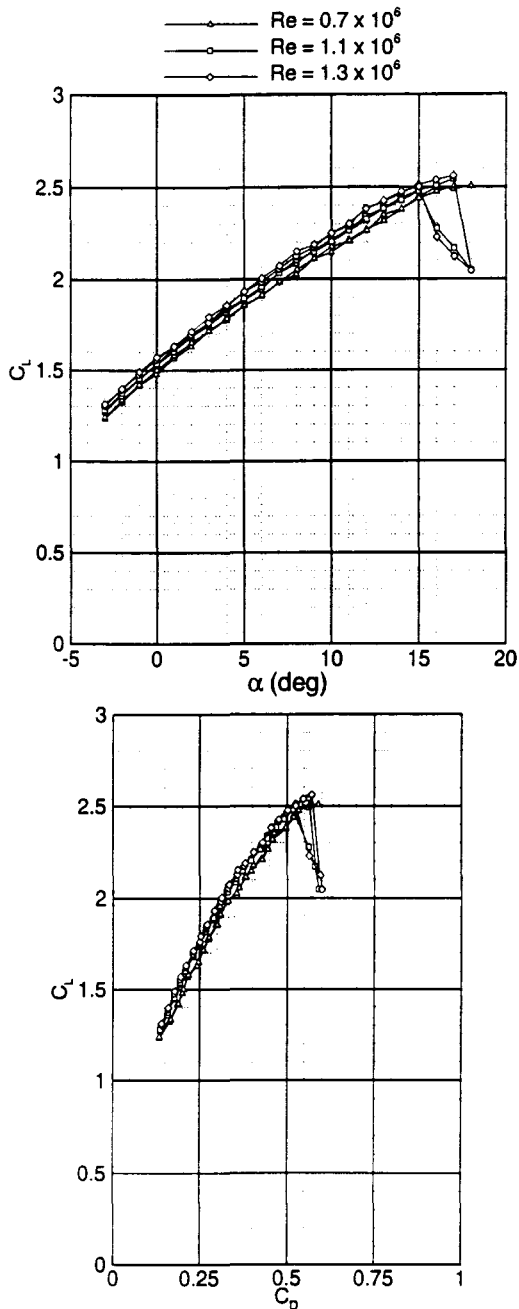


Figure 3.  $C_L$  vs.  $\alpha$  and  $C_L$  vs.  $C_D$  for UIUC700I at  $\delta_f=14$  deg and  $h/c=0.3$ .

Downstream flowfield measurements are summarized in Table 3. The aim of these measurements was to gain an understanding of the general flow structure behind the wing, including vortex development, and changes that would occur with varying the aforementioned parameters. The UIUC700I, Champ Car front wing, configuration was tested extensively, while a limited number of scans were performed with other configurations. The changes in the flowfield due to parameter changes such as angle of attack, Reynolds number, and flap deflection that occurred for the UIUC700I can be used to infer results for the other configurations.

Table 3. Seven-hole probe scan test matrix

| Configuration | $\alpha$ (deg) | Re                | $\delta_f$ (deg) |
|---------------|----------------|-------------------|------------------|
| UIUC700I      | 6              | $0.7 \times 10^6$ | 14               |
| UIUC700I      | 6              | $1.1 \times 10^6$ | 4, 14, 24        |
| UIUC700I      | 3, 6, 9        | $1.1 \times 10^6$ | 14               |
| UIUC700I      | 6              | $1.3 \times 10^6$ | 14               |
| UIUC700F      | 6              | $0.7 \times 10^6$ | 14               |
| UIUC700G      | 6              | $1.0 \times 10^6$ | 14               |
| UIUC700H      | 6              | $1.2 \times 10^6$ | 14               |

## RESULTS

**REYNOLDS NUMBER** – In a typical road or street course, race-car speeds may vary from as low as 50 mph to upwards of 200 mph. With this extreme change in conditions, performance of a wing can vary greatly. Therefore, it becomes important to quantify the effects that speed, or Reynolds number, has on performance of a race-car wing. Figure 3 shows the effect of Reynolds number on lift curves and drag polars for the UIUC700I configuration. As Reynolds number increases, lift coefficient increases and drag coefficient decreases. Typical increases in lift coefficient for an increase in Reynolds number from  $0.7 \times 10^6$  to  $1.1 \times 10^6$  averaged 2.5%, while an increase in Reynolds number from  $1.1 \times 10^6$  to  $1.3 \times 10^6$  caused an average increase in  $C_L$  of 1.9%. Decreases in total  $C_D$  for the same changes in Reynolds number were, on average, 2.3% and 1.2%, respectively. In the sense of an open-wheel race car, a desired effect would be a decrease in lift coefficient as speed (Re) increases, since high speeds typically occur on straightaways where downforce is not needed. From an aerodynamic standpoint, as the present data show, this is not likely with the current fixed-wing configurations allowed in open-wheel racing. An expected result is an increase in induced drag with higher speed, since the wing is operating at a higher lift coefficient. But the results show a reduction in overall drag coefficient. For this wing design the results indicate that the decrease in profile drag due to Reynolds number effects is larger than the associated increase in induced drag.

Figure 4 presents the downstream flowfield measurements for the UIUC700I configuration at  $\alpha = 6$  deg,  $\delta_f = 14$  deg, and  $Re = 1.1 \times 10^6$ . Note the formation of two large trailing vortices rolling up from the endplate edges, as well as a smaller vortex forming off of the "cutout." This smaller vortex is a result of the abrupt change in lift that occurs between the smaller chord root region and longer chord tip and does not appear in measurements taken with the UIUC700H, which had the Formula One flap. Downstream flow measurements for the UIUC700H configuration are presented in Figure 5. Data taken at  $Re = 0.7 \times 10^6$  and  $Re = 1.3 \times 10^6$  of the UIUC700I show no significant movement of the trailing vortex system. Also noticeable in the flowfield measurements, although not captured in the extents of Figures 4 and 5, is an interference region between the wing, tunnel floor, and ground plane.

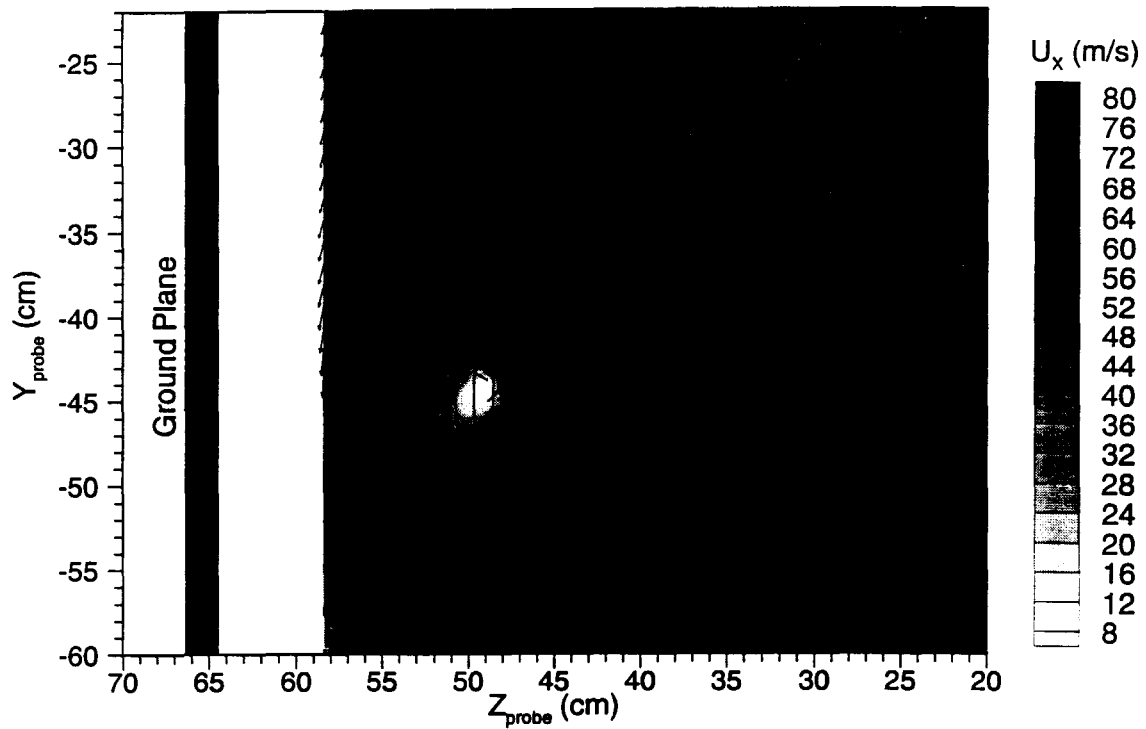


Figure 4. Downstream flowfield measurements for the UIUC700I at  $\alpha=6$  deg,  $\delta_t=14$  deg, and  $Re=1.1 \times 10^6$  as viewed from upstream of wing.

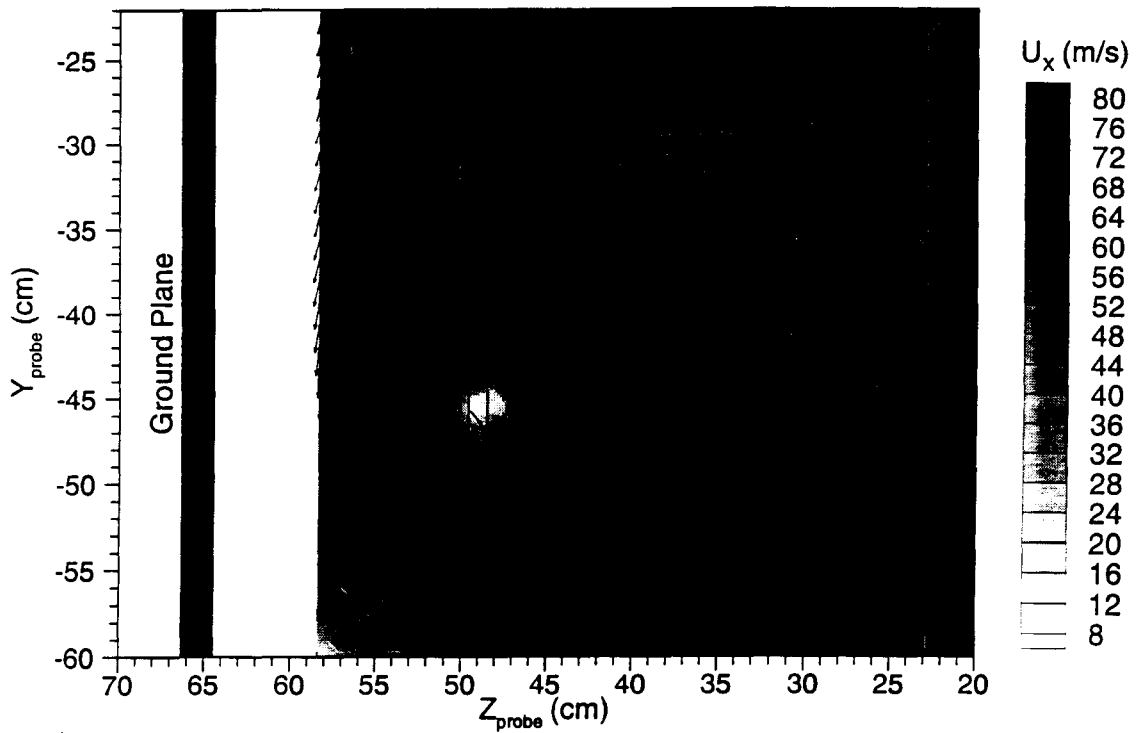
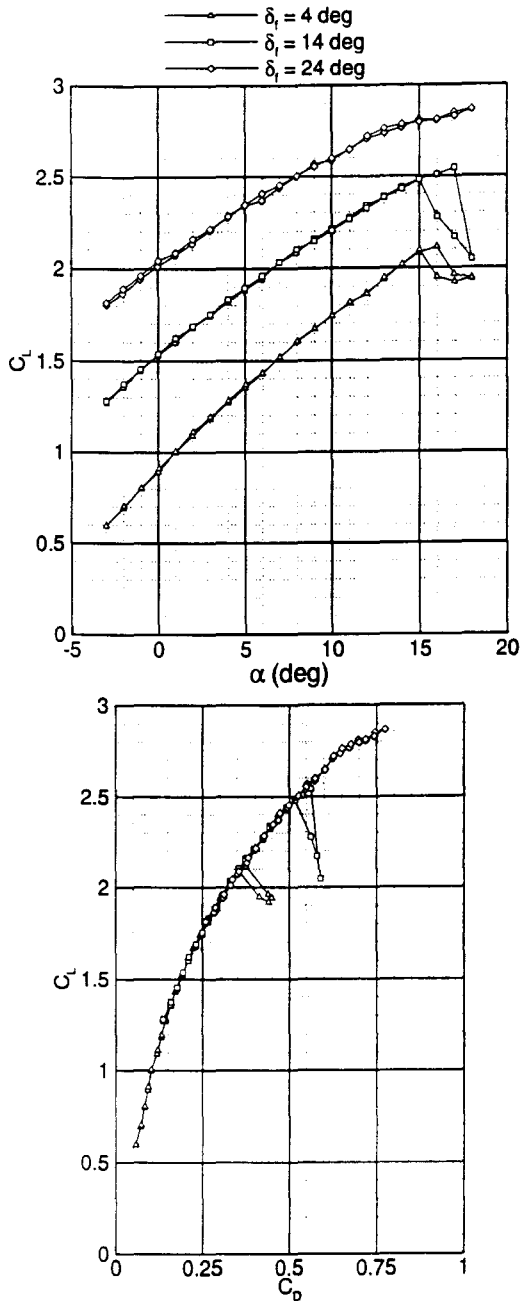


Figure 5. Downstream flowfield measurements for the UIUC700H at  $\alpha=6$  deg,  $\delta_t=14$  deg, and  $Re=1.2 \times 10^6$ , as viewed from upstream of wing.



**Figure 6.  $C_L$  vs.  $\alpha$  and  $C_L$  vs.  $C_D$  for UIUC700I at  $Re=1.1 \times 10^5$  and  $h/c=0.3$ .**

Due to clearance requirements between the seven-hole probe and the ground plane, measurements in this region are incomplete. Results on the overall flowfield structure due to this feature are unclear.

**FLAP DEFLECTION** – During a race, the ability to change the front-wing flap angle is the only way to adjust the aerodynamic performance of the car barring a complete change of the front nose cone, and hence changing the front wing completely. Therefore, the ability to quantify the effects of changing flap deflection on wing performance becomes extremely important. As listed in Table 2, each configuration was tested at flap deflections of 4, 14, and 24 deg. Figure 6 shows the lift curves and drag polars for the UIUC700I configuration at

$Re = 1.1 \times 10^5$  for these flap deflections. The average, minimum, and maximum increases in lift coefficient for each step change in flap deflection are summarized in Table 4. These results show that as flap deflection is increased by 10 deg, at a constant angle of attack, an average increase of 0.5 in lift coefficient occurs. Figure 6 also shows that although there is a large shift in the lift curves, there is no appreciable change in overall drag, when compared at a constant  $C_L$ . Because the values of overall drag are essentially constant at similar lift coefficients and constant Reynolds number, it is inferred that the changes in profile drag are small with respect to the overall drag, and that drag characteristics of a front wing are dominated by induced effects.

**Table 4. Increase in lift with changes in flap deflection of UIUC700I**

| Change in $\delta_f$ (deg) | Avg $\Delta C_L$ | Min $\Delta C_L$ | Max $\Delta C_L$ |
|----------------------------|------------------|------------------|------------------|
| 4 to 14                    | 0.5540           | 0.4492           | 0.6842           |
| 14 to 24                   | 0.4472           | 0.3685           | 0.5360           |

Figure 4 and Figure 7 show the flowfield measurements for the UIUC700I at  $\alpha = 6$  deg with flap deflections of 14 and 24 deg, respectively. Lift coefficients for these cases are 1.95 for  $\delta_f = 14$  deg and 2.37 for  $\delta_f = 24$  deg. Comparison of these plots show that the trailing vortex from the suction side of the wing at the endplate moves closer to the root by approximately 1.2 cm, as well as 1.2 cm further from the ground. The movement of the vortex with increasing flap deflection has two competing effects. First, the increased lift at high flap deflections will cause more induced drag, requiring more engine power and decreasing top speed. Alternatively, more flow might be forced through the underbody because of the vortex being moved closer to the root of the car. An increase in flow to the underbody channels of a race car, particularly in a Champ Car, will manifest itself as an increase in downforce, and higher cornering speeds can be achieved. The wing/floor/ground-plane interaction region, not fully captured in Figure 7, also appeared to grow with increasing flap deflection. This is likely due to the higher speeds over the suction side of the wing that result from the increased loading provided by the flap deflection increase. Since the complete area of this flow was not captured in the seven-hole probe scans, it is not known how this affects the rest of the flowfield.

**FLAP PLANFORM** – In addition, the effect of flap planform was compared. Here, the two different flap planforms were tested with the same endplate. Comparisons were made between the UIUC700I and UIUC700H, both having the Champ Car front endplate, and the UIUC700F and UIUC700G, both having the Formula One-style front endplate. Lift and drag data for the I and H configurations are shown in Figure 8, while selected pressure distributions over the main element for both configurations are shown in Figure 9. Results for the UIUC700F and G comparison are not shown, but are

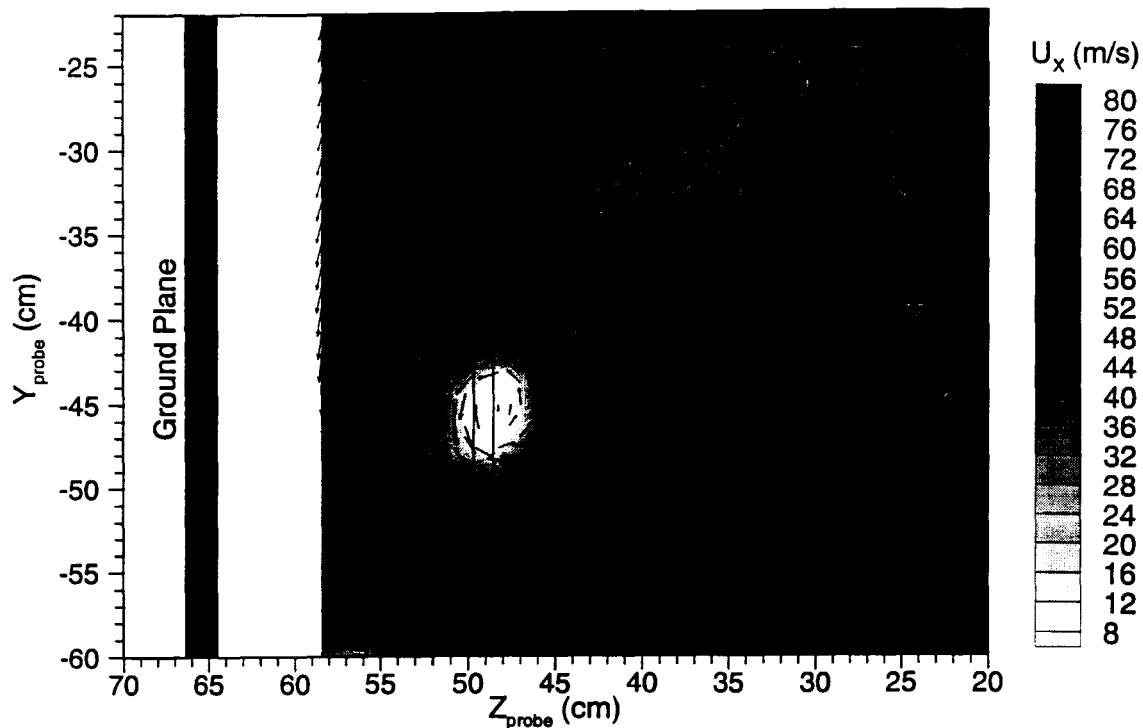


**Figure 7. Downstream flowfield measurements for the UIUC700I at  $\alpha=6$  deg,  $\delta_f=24$  deg, and  $Re=1.1 \times 10^6$ , as viewed from upstream of wing.**

consistent with the UIUC700I and H configurations. As a result of increasing the wing planform area by 4.5%, the average increase in  $C_L$  is 0.15 over the range of angles of attack tested. This effect, however, is not explained by the increase in area. At first glance, it might be expected that an increase in area without an increase in span would result in higher induced drag and lower lift coefficients, which are results of increased aspect ratio. But Figure 8 shows that an increase in  $C_L$  occurs. This is largely in part due to the increase in local chord that occurs over much of the flap. The main element can be loaded more because of this, and as a result lift coefficient is increased. Examination of the pressure distributions of Figure 9 confirms this result. The drag polar of Figure 8 also shows that there is no significant effect on overall drag due to a change in wing planform, suggesting that planform does not have a large effect on induced drag.

The downstream flowfield measurements for the UIUC700H are shown above in Figure 5. Comparing these measurements with those for the UIUC700I (see Figure 4), it is seen that the suction side vortex is stronger, moves closer to the root and further from the ground with the Formula One-style flap (UIUC700H). An increase in induced drag would be the expected result; however, no significant increase is shown.

**ENDPLATE PLANFORM** – The overall effect that endplate planform area has on performance of the front wing is, perhaps, the most interesting. Although racing cars in both CART (Champ Car) and Formula One are extremely restrictive in terms of endplate size and position, it is still essential that a car manufacturer maximize performance. Figure 10 compares the

UIUC700F with the UIUC700H, both having the Formula One flap and Formula One and Champ Car front-wing endplates, respectively. When the Champ Car endplate was used, lift coefficient increased by an average of 0.0958 at constant  $\alpha$ , while drag coefficient at constant  $C_L$  decreased by an average of 13.7%. Hence, adding endplate area produces a more efficient wing. This effect can also be partially explained by the positioning of the wing within the endplate. It is difficult to separate the two without further study. As shown in Figure 1, the positioning of the wing is closer to the edge of the Formula One endplate than with the Champ Car front endplate. The lack of endplate area between the wing's suction surface and the freestream allows the trailing vortex to roll-up earlier, which can result in more induced drag and less lift.

## CONCLUSION

The results from this study show that many defining parameters in the design and setup of open-wheel race-car front wings have a significant effect on performance. Reynolds number effects were least significant, with changes in lift and drag of typically 3-4% over the Reynolds number range tested. Changes in flap deflection of 10 deg, caused an average increase in  $C_L$  of 0.5, while drag coefficient was largely unaffected at a constant lift coefficient. A study of changes in flap planform show significant increases in lift. This is largely due to the increased loading that occurs on the main element. Changing endplate planform reveals that endplate design is quite significant in determining the performance of a race-car front wing. When endplate area is increased, overall lift coefficient increases while there is a significant reduction in drag coefficient.

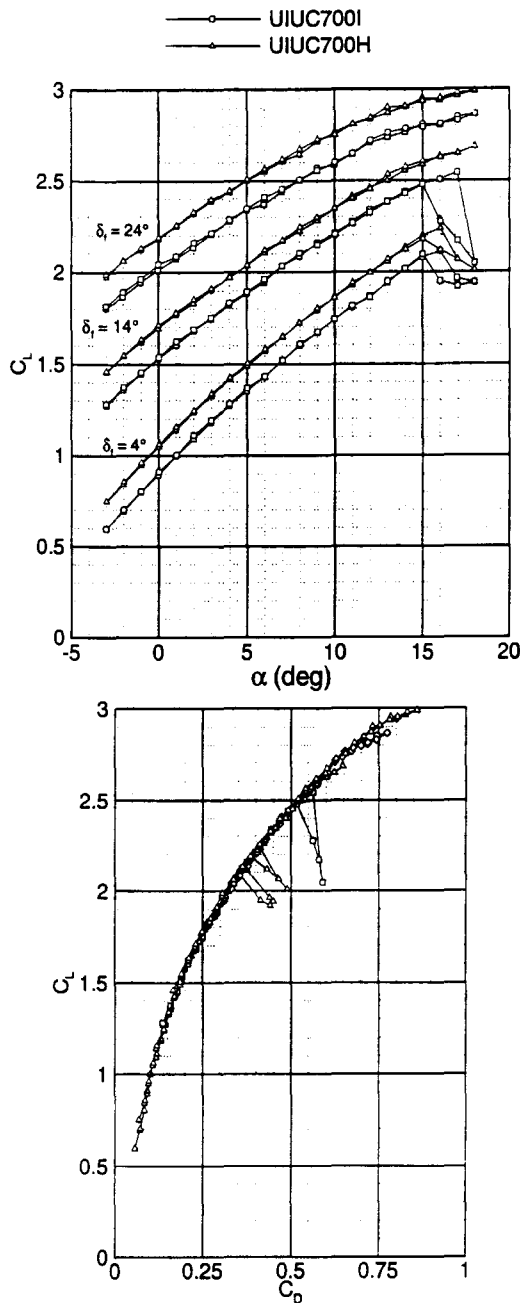


Figure 8.  $C_L$  vs.  $\alpha$  and  $C_L$  vs.  $C_D$  for UIUC700I and UIUC700H at  $Re=1.1 \times 10^6$  and  $h/c=0.3$ .

#### ACKNOWLEDGMENTS

The support of Ford Motor Company, AVT Motorsports Technology Group with technical monitors John LaFond, Paul Carrannanto, and Fredrico Hsu is gratefully acknowledged. Also, the early input of Frank Hsu leading to the initiation of this work is greatly appreciated. The efforts of Mark Allen and Yvan Tinel in the construction of the wind tunnel models are also greatly appreciated. Additional recognition is extended Andy Broeren for his helping hand throughout the various stages of this project. Much of this research could not have been performed without his valuable input and effort.

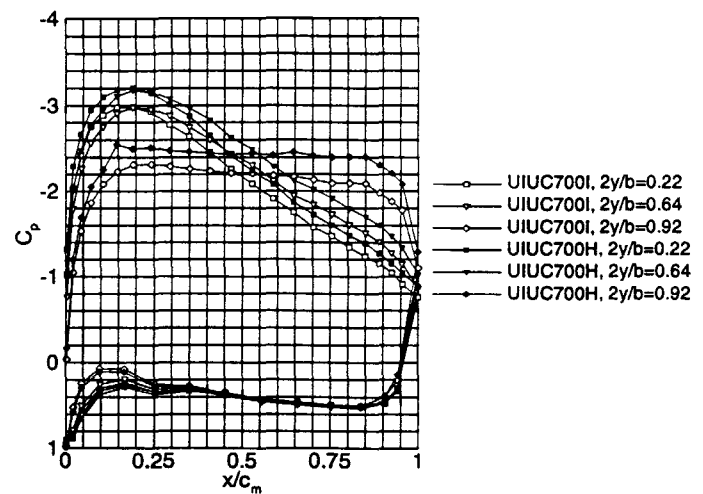


Figure 9. Main element pressure distributions for UIUC700I and UIUC700H at  $\alpha=6^\circ$ ,  $\delta_r=14^\circ$ ,  $Re=1.1 \times 10^6$ , and  $h/c=0.3$ .

#### ABOUT THE AUTHORS

William J. Jasinski performed this research while he was a Graduate Research Assistant at the University of Illinois. He currently is an Experimental Engineer at the General Motors Corporation Design Center, MC480-113-PB6, 30100 Mound Road, Box 9030, Warren, Michigan 48090-9030.

Michael S. Selig is an Associate Professor at the University of Illinois Department of Aeronautical and Astronautical Engineering, 306 Talbot Laboratory, 104 South Wright Street, Urbana, Illinois 61801.

#### REFERENCES

- Hurst, D.W., "Modern Wind Tunnel Testing of Indycars," SAE Paper 942497, 1994 *Motorsports Engineering Conference Proceedings, Vol. 1*, pp. 151-159, December 1994.
- Katz, J., "Aerodynamic Model for Wing-Generated Down Force on Open-Wheel-Racing-Car Configurations," SAE Paper 860218, February 1986. *SAE Transactions*, Vol. 95, pp. 129-137, 1986.
- Coiro, D.P., F. Nicolosi, A. Amendola, D. Barbagallo, L. Paparone, S. Beccio, P. Castelli, and S. Limone, "Experiments and Numerical Investigation on a Multi-Component Airfoil Employed in a Racing Car Wing," SAE Paper 970411, *Topics in Vehicle Aerodynamics*, pp. 221-231, 1997.
- Berchak, M.J. and Camosy, M.W., "Comparison of Full-Scale Wing Wind Tunnel Test to Scale-Model Test for Open Wheel Race Cars," SAE Paper 942495, 1994 *Motorsports Engineering Conference Proceedings, Vol. 1*, pp. 141-149, December 1994.
- Ranzenbach, R. and Barlow, J.B., "Two-Dimensional Airfoil in Ground Effect, An Experimental and Computational Study," SAE Paper 942509, 1994 *Motorsports Engineering Conference Proceedings, Vol. 1*, pp. 241-249, December 1994.
- Ranzenbach, R. and Barlow, J.B., "Cambered Airfoil in Ground Effect - An Experimental and Computational Study," SAE Paper 960909, 1996 *Motorsports Engineering Conference Proceedings, Vol. 1*, pp. 269-276, December 1996.

7. Ranzenbach, R., Barlow, J.B., and Diaz, R.H., "Multi-Element Airfoil in Ground Effect - An Experimental and Computational Study," AIAA Paper 97-2238, June 1997.
8. Gopalarathnam, A., Selig, M.S. and Hsu, F., "Design of High-Lift Airfoils for Low Aspect Ratio Wings with Endplates," AIAA Paper 97-2232, June 1997.
- Noe, S.C., "Force Balance Measurements of Wind-Turbine Airfoil Performance with Simulated Leading-Edge Ice Accretions," Master's Thesis, University of Illinois at Urbana-Champaign, August 1996.
10. Jasinski, W.J., Noe, S.C., Selig, M.S. and Bragg, M.B., "Wind Turbine Performance Under Icing Conditions," *Journal of Solar Energy Engineering*, Vol. 120, No. 1, February 1998, pp. 60-65.
11. Rediniotis, O.K., Hoang, N.T. and Telionis, D.P., "The Seven-Hole Probe: Its Calibration and Use," *Forum on Instructional Fluid Dynamics Experiments*, Vol. 152, pp. 21-26, June 1993.
12. Zilliac, G.C., "Calibration of Seven-Hole Pressure Probe For Use in Fluid Flows with Large Angularity," NASA TM 102200, Decemeber, 1989.

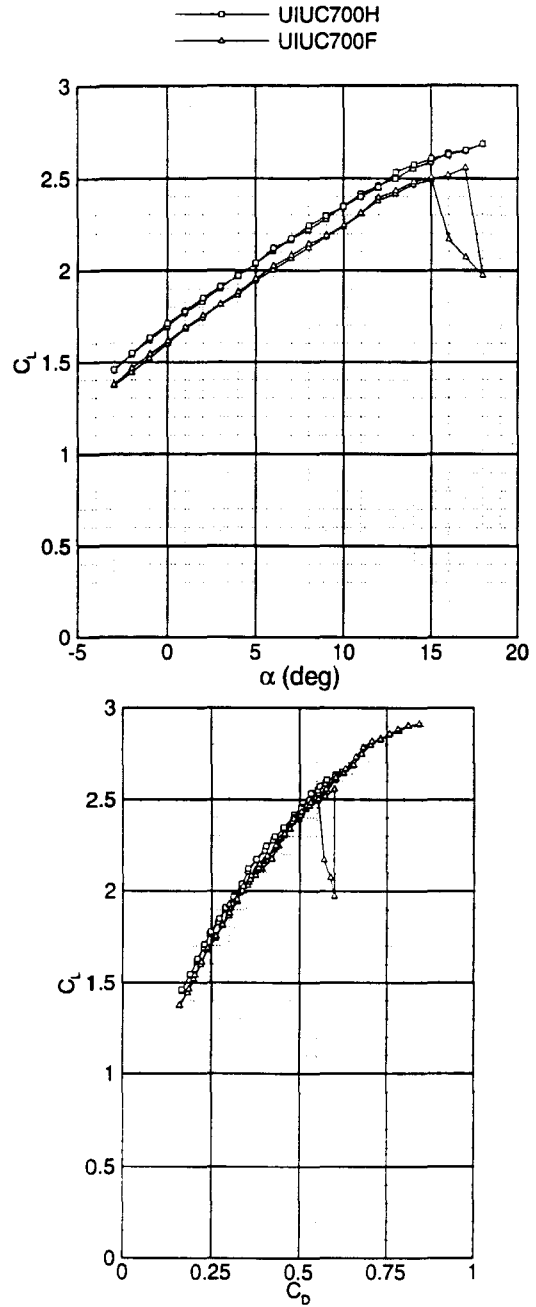


Figure 10.  $C_L$  vs.  $\alpha$  and  $C_L$  vs.  $C_D$  for UIUC700F and UIUC700H at  $\delta_T=14$  deg,  $Re=1.1 \times 10^6$ , and  $h/c=0.3$ .